Influence of Ultrasonic-Shot Peening on Bending Fatigue of TiNi Shape Memory Alloy

Kohei Takeda†, Ryosuke Matsui† and Hisaaki Tobushi†

Abstract The fatigue property of shape memory alloy (SMA) is one of the most important subjects in view of evaluating functional characteristics of SMA elements. In the present study, ultrasonic shot peening (USP) was applied to induce compressive residual stress on the surface layer of TiNi SMA tape and the influence of USP on the bending fatigue life was investigated. The fatigue life of USP-treated tape is longer than that of the as-received tape. The fatigue life of the tape USP-treated with high coverage is longer than that with low coverage. The fatigue life of the USP-treated tape increases in proportion to the hardness on the surface of the tape.

1. Introduction

The shape memory alloy (SMA) is expected to be applied as intelligent material since it shows the unique characteristics of the shape memory effect and superelasticity [1]. The TiNi SMAs are among the best SMAs since the fatigue life is longer, the recoverable strain is larger and the corrosion resistance is higher than other SMAs. With respect to the fatigue properties, the fatigue tests in tension and rotating bending have been conducted [2-4]. However, the plane-bending deformation is used in practical applications. In the growing number of TiNi SMA applications, these materials should fulfill high requirements of fatigue, corrosion and wear resistance. On the other hand, the application of SMA has some limitations, particularly in thermomechanical cyclic loading cases. If the maximum strain is large, mechanical property can change during cycling and structural components can be damaged due to fatigue under high cycles [5-6]. In these cases, fatigue of SMA is one of the important properties in view of evaluating functional characteristics as SMA elements.

It is known that the shot peening is used to induce compressive residual stresses on the surface layer of metallic parts [7]. The residual stresses produced increase the fatigue performances. The ultrasonic shot peening (USP) has the following advantages: (1) saving space since cabinet and dust collector are not needed, (2) clean operation lines with improved operation environment (dust and noise) because of no dust collector used in lines and (3) shot peening effect with the same or higher compressive residual stress compared to conventional shot peening and with the better surface finishing than conventional shot peening [8]. It is suggested that USP would produce SMA elements with a longer working life. The study on enhancement of the fatigue life for TiNi SMA by USP has not been investigated till now. In particular, since impressions appear little by USP in the region of superelasticity, the influence of USP on the fatigue life is not clear.

In this paper, we report and discuss the influence of USP shot media diameter and coverage on the bending fatigue life of TiNi SMA tape which shows superelasticity.

2. Experimental Procedure

The materials used in the experiment were Ti-50.85at%Ni tapes with a thickness of 1 mm and a width of 2.5 mm. The length of the tapes was 100 mm for the tension test and 80 mm for the fatigue test. They were polycrystalline, produced by Furukawa Techno Material Co., Ltd. and applied to an element of a brassiere. The tapes were heat-treated at 803 K for 10 min in air followed by water quench. The material shows superelasticity at room temperature.

† Department of Mechanical Engineering, Aichi Institute of Technology

In order to investigate the influence of USP on the fatigue life, the tapes were USP-treated. In order to investigate the influence of surface roughness on the fatigue life, the surface of the tape in one group was polished by using the abrasive paper No 1000, 1200, 1500, 2000, 2500 and then finished using 0.04 micron SiO2 colloidal suspension.

The specimen were divided into the following groups: (1) as-received, (2) polished and (3) three kinds of USP-treated tapes.

One end of a TiNi SMA tape was gripped during USP treatment. Both flat surfaces of the tape were shot-peened from two opposite directions by steel balls as shot media. The shot media was an SUJ2 steel ball with Vickers hardness *HV* of 850 used for a miniature bearing. Diameters of the steel balls used were 0.8 mm and 1.2 mm. USP was carried out using the ultrasonic equipment produced by SONATS (Toyo Seiko Co., Ltd.). The frequency of the vibrating sonotrode was 20 kHz. The impressions do not clearly appear on the shot-peened surface of the superelastic SMA. In order to specify the peening intensity of USP, Almen test strips were used. The coverage was obtained as follows: (1) the time of the USP-treatment for Almen test strips to the coverage of 100% was measured at first, and (2), in the case of coverage of 2000%, the USP-treatment was applied to the SMA tape for 20 times longer time than that of the coverage of 100%. Coverages applied were 2000% and 4000%. In the test to investigate the influence of the shot media diameter on the fatigue properties, two diameters of 0.8 mm and 1.2 mm were used for a coverage of 2000%. In the test to discuss the influence of the coverage, two coverages of 2000% and 4000% were applied for a shot media diameter of 0.8 mm.

In the tension test, displacement was measured by an extensometer with a gauge length of 50 mm for SMA tapes. Strain ε was determined by nominal strain. The tension test was carried out under a constant strain rate $d\varepsilon / dt = 1.67 \times 10^{-4}$ s^{-1} in air at room temperature T_r.

In the fatigue test, an alternating-plane bending fatigue test machine [9] was used. The test for alternating-plane bending fatigue was carried out in air at room temperature. The maximum bending strain appeared on the flat surface of the SMA tape at which USP was applied. The frequency of cyclic bending was found to be 2.5 Hz (150 cpm). Temperature of the specimen surface at the midpoint of two grips, where the maximum bending strain appeared, was measured by a thermocouple during the alternating-plane bending fatigue test.

A scanning electron microscope (SEM) was used to observe the fracture surface of the specimen.

A laser microscope VK-X200 made by Keyence Co. was used to observe the surface roughness of the specimen.

The Vickers hardness test machine was used to observe the surface hardness of the specimen. The indentation load was 49 N.

The residual stress was measured by X-ray diffraction using 2θ-$\sin^2\psi$ diagrams for the (211) plane of the austenite phase.

3. Results and Discussion

3.1 Tensile deformation property

The stress-strain curves of four kinds of SMA tapes obtained by the tension test are shown in Fig. 1. All stress-strain curves draw hysteresis loops during loading and unloading, showing the superelasticity. The upper stress plateau during loading appears due to the stress-induced martensitic transformation (SIMT). In the stress plateau region, the transformation band progresses due to the SIMT in TiNi SMA tape [10]. The lower stress plateau during unloading appears due to the reverse transformation. The martensitic transformation start stress σ_{MS} was obtained from the intersection of two straight lines: the initial elastic part and the upper stress plateau part. Values of σ_{MS} are 370 MPa, 380 MPa, 400 MPa and 410 MPa for the as-received tape, the tape USP-treated with shot media diameter d = 0.8 mm and coverage c = 2000%, that with d = 1.2 mm and c = 2000%, and that with d = 0.8 mm and c = 4000%, respectively. The value of σ_{MS} increases slightly by USP since the influence of USP appears only on the shot-peened surface layer of the tape. Although both the shot media diameter d and coverage c affect the value σ_{MS}, the influence of coverage c is a little higher than that of shot media diameter d.

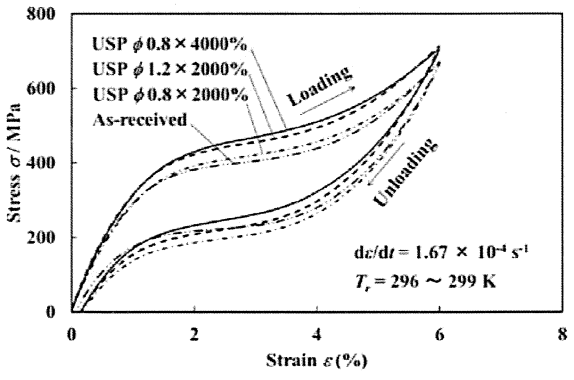

Fig. 1 Stress-strain curves

3.2 Bending Fatigue Property

3.2.1 Fatigue life

(1) Fatigue life curve

The relationships between the bending strain amplitude ε_a and the number of cycles to failure N_f for five kinds of tapes obtained by the alternating-plane bending fatigue test under a constant frequency f = 150 cpm at room temperature are shown in Fig. 2. The bending strain amplitude ε_a was obtained from the bending strain on the surface of the specimen at the fracture point. The specimen was fractured at the midpoint of two grips. As can be seen in Fig. 2, the larger the bending strain amplitude, the shorter the fatigue life is. The fatigue life of polished and shot-peened tapes is longer than that of the as-received tape. The fatigue life of the tape USP-treated with d = 0.8 mm and c = 2000% is almost the same as that with d = 1.2 mm and c = 2000%. The fatigue life of the tape USP-treated with d = 0.8 mm and c = 4000% is longer than that of other shot-peened tapes. The fatigue life of the tape USP-treated with d = 0.8 mm and c = 4000% is 2.6 times at ε_a = 3% and 10 times at ε_a = 1% longer than that of as-received tape, respectively.

The relationships between the bending strain amplitude ε_a and the number of cycles to failure N_f shown on the logarithmic graph are almost expressed by straight lines for all materials. The relationship therefore can be expressed by a power function as follows:

$$\varepsilon_a \cdot N_f^{\beta} = \alpha \qquad (1)$$

where α and β represent ε_a in N_f = 1 and the slope of the log ε_a - log N_f curve, respectively. The values of α and β are 1.16 and 0.55 for the as-received tape, 1.68 and 0.55 for the polished tape, 0.52 and 0.41 for both tapes USP-treated with d = 0.8 mm at c = 2000% and with d = 1.2 mm at c = 2000%, and 0.37 and 0.33 for the tape USP-treated with d = 0.8 mm at c = 4000%, respectively. The calculated results of Eq. (1) are shown by solids lines in Fig. 2. The overall inclinations are well approximated by the solid lines.

(2) Temperature rise

As observed in Fig. 2, the larger the bending strain amplitude, the shorter the fatigue life is. During cyclic bending, SMA is subjected to exothermic martensitic transformation repeatedly. Therefore, temperature of the material increases markedly in the early 20 - 30 cycles and is saturated in a certain value thereafter [11]. The difference between the saturated temperature T_s and room temperature T_r is defined as the saturated temperature rise $\Delta T_s = T_s - T_r$. The relationships between the saturated temperature rise ΔT_s and the bending strain amplitude ε_a for four kinds of tapes obtained from the test at room temperature T_r are shown in Fig. 3. In Fig. 3, the data obtained are plotted by several symbols for each tape. The region, where the data are plotted, is shaded. Temperature rise ΔT_s increases in proportion to ε_a for all tapes and the difference of ΔT_s is slight among four tapes. As seen in Fig. 1, the stress-strain curve of the tape draws a hysteresis loop during loading and unloading. The area surrounded by the hysteresis loop corresponds to the dissipated work per unit volume W_d [12]. The dissipated work W_d is evaluated by the product of the difference $(\sigma_M - \sigma_A)$ between the upper plateau stress σ_M and the lower plateau stress σ_A and the martensitic transformation strain range ε_M. The dissipated work W_d of the surface element with the bending strain amplitude ε_a is estimated by the following equation [13]

$$W_d = (\sigma_M - \sigma_A)(\varepsilon_a - \varepsilon_{MS}) \qquad (2)$$

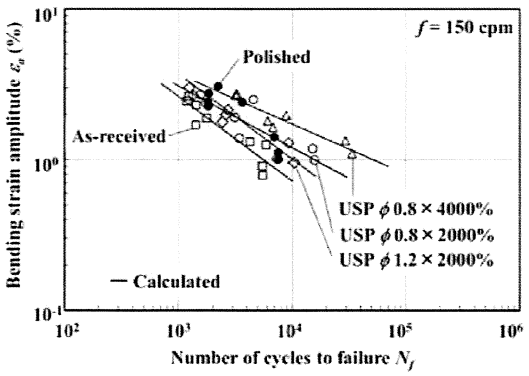

Fig. 2 Relationship between bending strain amplitude and the number of cycles to failure.

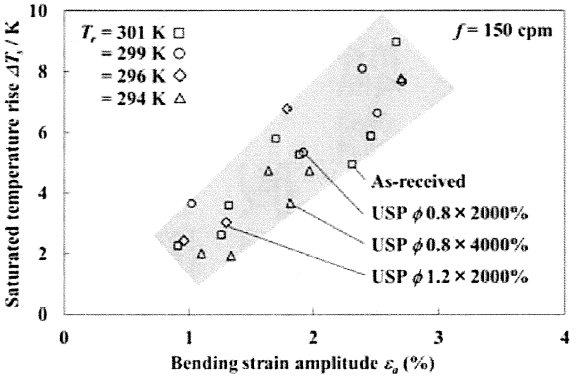

Fig. 3 Relationship between saturated temperature rise ΔT_s and bending strain amplitude ε_a.

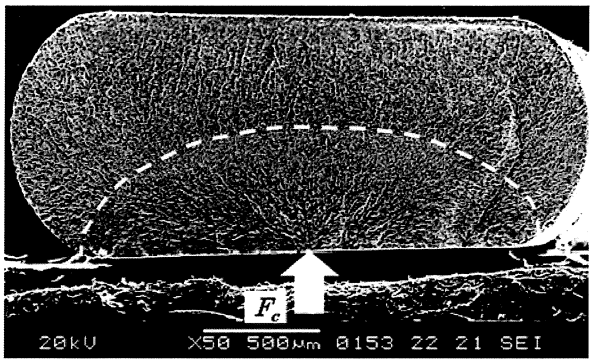

Fig. 4 SEM photograph of fracture surface of as-received tape for ε_a = 1.26% and N_f = 5906.

where ε_{MS} denotes the martensitic transformation start strain. Therefore, if ε_a is large, W_d is large, and as a result large amount of heat is generated. This is the reason why ΔT_s increases in proportion to ε_a. In SMAs, σ_M increases in proportion to temperature as follows: $d\sigma_M / dT = C_M$ and C_M = 6 MPa/K for TiNi SMA [14]. It should be noticed that, if ΔT_s is large, σ_M increases. Therefore, in the practical application of SMA elements, high σ_M induced due to temperature rise ΔT_s under cyclic bending causes large fatigue damage, that is, the fatigue crack nucleates earlier and the fatigue crack propagate rate becomes higher, resulting in short fatigue life.

3.2.2 Fatigue crack

(1) Fatigue surface

In the case of as-received tapes, the fatigue crack initiates at the central part of the flat surface subjected to maximum bending strain. In the case of USP tapes, the fatigue crack initiates at the corner different from the flat surface subjected to maximum bending strain. Let us discuss the influence of USP on the fatigue crack initiation and the fatigue crack growth by observing the fracture surface.

(i) As-received material

Figure 4 shows the SEM photograph of a fracture surface of the as-received tape obtained by the fatigue test for ε_a = 1.26 %. In Fig. 4, F_c denotes the point of the fatigue crack initiation. The crack nucleates at a certain point F_c in the central part of the flat surface of the tape and propagates toward the center in a sinuous radial pattern. Although small cracks are observed in both flat surfaces of the tape subjected to maximum bending strain, one single crack grows preferentially. Following the appearance of fatigue crack with a semi-elliptical surface, unstable fracture finally occurs. In the case of as-received tapes, the point F_c appears at a central part of the flat surface subjected to the maximum bending strain and the fatigue life is short.

(ii) USP material

SEM photographs of a fracture surface for the USP tape in the case of a bending strain amplitude ε_a = 1.64% are shown in Fig. 5. The tape was USP-treated with shot media diameter d = 0.8 mm and coverage c = 4000%. The whole fracture surface, the fracture surface at the crack initiation part (1), the fracture surface in the middle part of unstable fracture region (2), and the fracture surface in the final unstable fracture part (3) located on the opposite side of the crack initiation part (1) are shown in Figs. 5 (a), 5 (b), 5 (c) and 5 (d), respectively.

As can be seen in Figs. 5 (a) and 5 (b), the fatigue crack nucleates at a certain point F_c in the corner (1) on the side surface near the flat surface of the tape and propagates toward the center in a sinuous radial pattern. The distance from the flat surface of the tape to the crack initiation point F_c is 40 μm. Although small cracks are observed on four corner surfaces of the tape, one single crack grows preferentially. The reason why the fatigue crack nucleates at the corner surface is as follows. Although the maximum bending strain appears on the flat surface of the tape, the flat surface is subjected to USP and therefore it is hard for the fatigue crack to nucleate on the flat surface. The side surface of the tape is subjected to slight USP. As a result, the fatigue crack nucleates at the corner F_c near the flat surface. This phenomenon is similar to the fatigue crack initiation point of a TiNi SMA wire subjected to nitrogen-ion implantation [15]. In the case of an ion-implanted wire, the fatigue crack nucleates at a certain point different from the maximum bending strain point where the maximum amount of nitrogen ion was implanted. In practical applications of SMAs, the fatigue life of SMA elements increases if USP is treated not only on the surface at the maximum stress point but also on the surface in the region near the maximum stress point.

As can be seen in Fig. 5 (a), following the appearance of fatigue fracture with a quarter-elliptical surface, unstable fracture finally occurs. As can be seen in Fig. 5 (c), isometric dimples with an average diameter of about 3 μm appear in the middle part of unstable fracture region (2). As seen in Fig. 5 (d), elongated dimples are found distributed in the direction parallel to the flat surface according to the propagation of the crack induced by tearing in the final unstable fracture part (3).

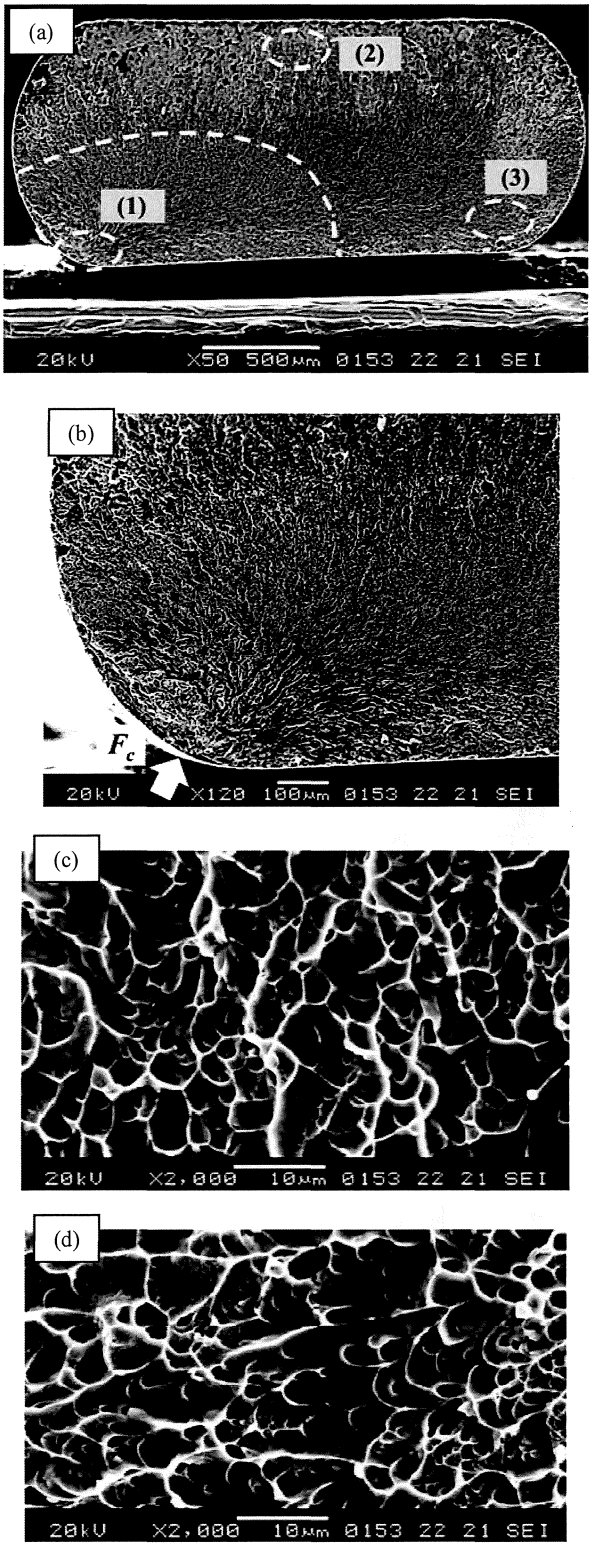

Fig. 5 SEM photographs of fracture surface of USP tape with d = 0.8 mm and c = 4000% for ε_a = 1.64% and N_f = 6788: (a) whole fracture surface, (b) crack initiation part (1), (c) middle part of unstable fracture (2), and (d) final unstable fracture part (3).

(2) Fatigue crack growth

(i) Fatigue crack growth area

Let us discuss the fatigue crack growth area A_f which is surrounded by dashed semi-elliptical or quarter-elliptical lines shown in Figs. 4 or 5(a). The relationships between the fatigue crack growth area A_f and the bending strain amplitude ε_a for four kinds of tapes obtained by the fatigue test are shown in Fig. 6. In Fig. 6, the data obtained are plotted by several symbols for each tape. The regions, where the data are plotted, are shaded separately for the USP tape with d = 0.8 mm at c = 4000 % and for other three tapes. As can be seen in Fig. 6, only the area A_f of the USP tape with d = 0.8 mm at c = 4000 % is larger than that of other three tapes. The larger the bending strain amplitude, the smaller the fatigue crack growth area is. If the bending strain amplitude is large, the fatigue crack growth area is small, resulting in a short fatigue life. In the case of USP with d = 0.8 mm at c = 4000%, A_f is larger than other three conditions, which corresponds to the longer fatigue life.

(ii) Fatigue crack growth length

As observed in Figs. 4 and 5, the fatigue fracture surface shows a semi-elliptical or a quarter-elliptical form. Let us discuss the fatigue crack growth length along the flat surface a_s from the crack initiation point F_c and that toward the center a_c. The dependence of a_s and a_c on the bending strain amplitude ε_a is shown in Fig. 7. In Fig. 7, the data of a_s are plotted by closed symbols and those of a_c by open symbols, respectively. The regions, where they are plotted, are shaded. As can be seen, the larger the bending strain amplitude ε_a, the smaller the crack growth length a_s is. The dependence of a_c on ε_a is slight. Values of a_c are around 0.5 mm, a half of a thickness of the tape of 1 mm. Values of a_s are larger than those of a_c since the bending

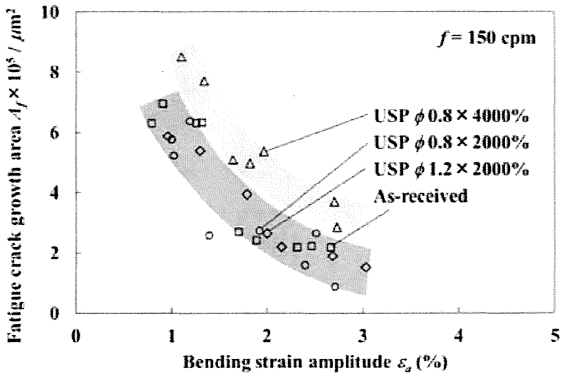

Fig. 6 Relationship between fatigue crack growth area and bending strain amplitude.

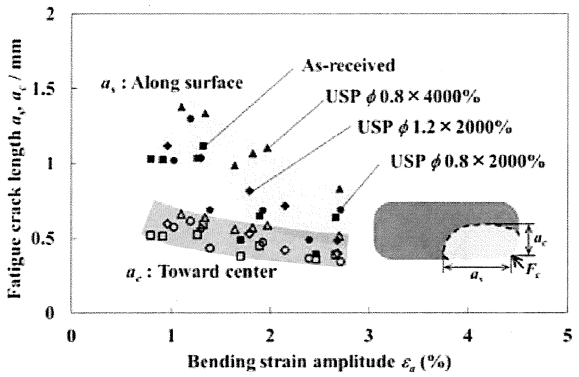

Fig. 7 Dependence of fatigue crack lengths a_s and a_c on bending strain amplitude: a_s is shown by closed symbols and a_c by open symbols.

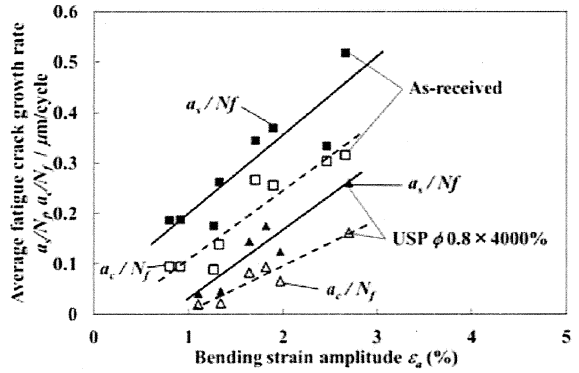

Fig. 8 Dependence of average fatigue crack growth rates a_s/N_f and a_c/N_f on bending strain amplitude ε_a for as-received tape and USP tape with d = 0.8 mm and c = 4000% : a_s/N_f is shown by closed symbols and a_c/N_f by open symbols.

strain is largest on the flat surface of the tape and is small in the central part of the tape.

(iii) Average fatigue crack growth rate

The dependence of average fatigue crack growth rate till fracture along the flat surface a_s/N_f and that toward the center a_c/N_f on the bending strain amplitude ε_a for as-received tape and the tape USP-treated with d = 0.8 mm at c = 4000% is shown in Fig. 8. In Fig. 8, the data of a_s/N_f are plotted by closed symbols and those of a_c/N_f by open symbols, respectively. As can be seen, the larger the bending strain amplitude, the larger the crack growth rates are. The average fatigue crack growth rates for the as-received tape are higher than those for the USP tape. This means the fact that the average fatigue crack growth rates decrease by the USP treatment, resulting in longer fatigue life.

3.2.3 Influence of hardness on fatigue life

Vickers hardness of the surface for four kinds of tapes was measured by a load of 49 N. The relationships between the number of cycle to failure N_f and Vickers hardness HV for various values of bending stain amplitude ε_a are shown in Fig. 9. In Fig. 9, the data are plotted by several symbols and the relation for each ε_a is connected by the straight line. As can be seen in Fig. 9, the fatigue life N_f of TiNi SMA treated by USP increases in proportion to Vickers hardness HV as same as normal metals. The influence of HV on N_f is slight in the case of large ε_a. The relationships shown on the semi-logarithmic graph are almost expressed by straight lines for each ε_a. The relationship therefore can be expressed by the following equation.

$$\log N_f = \log a + bHV \tag{3}$$

where a and b represent N_f in HV = 0 and the slope of the log N_f – HV curve, respectively. The value of b denotes the sensibility of influence of HV on the N_f. The a denotes the value of N_f unaffected by HV. The fatigue life N_f can be expressed by an exponential function of HV from Eq. (3) as follows:

$$N_f = a \exp(\ln 10 \cdot bHV) \tag{4}$$

The coefficients a and b can be expressed by the linear functions of ε_a as follows:

$$a = a_1 \varepsilon_a + a_2$$
$$b = b_1 \varepsilon_a + b_2 \tag{5}$$

where a_1 and b_1 represent the slopes of the $a - \varepsilon_a$ curve and $b - \varepsilon_a$ curve, and a_2 and b_2 represent a and b in ε_a = 0, respectively. The values of a_1, a_2, b_1 and b_2 are -86.5, 32.6, -0.0988 and 0.00738, respectively. The results calculated from Eqs. (4) and (5) are shown by solid lines in Fig. 9. The overall inclinations are well-approximated by the solid lines.

3.2.4 Surface roughness

It is known that surface roughness of the material affects the fatigue life. If the surface is rough, the fatigue life is short [16]. As observed in Fig. 2, the fatigue life of the polished tape is longer than the as-received tape. In order to investigate the influence of surface roughness on the fatigue life, surface roughness was measured.

Arithmetic mean roughness R_a for five kinds of tapes is shown in Fig. 10. The value of R_a for the as-received tape is 0.65

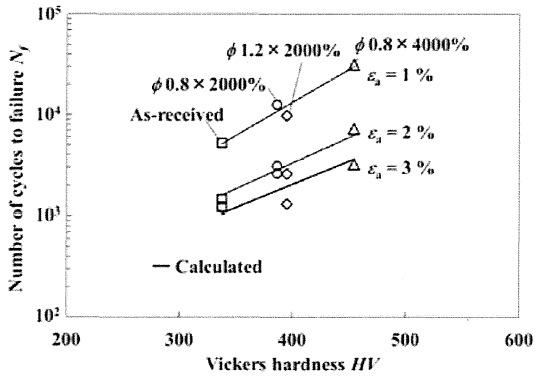

Fig. 9 Relationship between number of cycles to failure and Vickers hardness for various strain amplitudes ε_a.

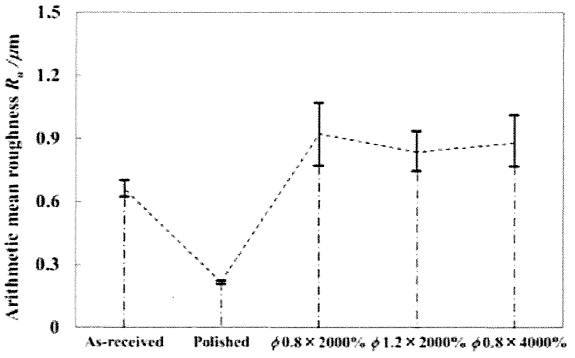

Fig. 10 Arithmetic mean surface roughness for five kinds of tapes.

μm. The value of R_a = 0.2 μm for the polished tape is about one-third as large as the as-received tape. As observed in Fig. 2, the fatigue life of the polished tape is longer than that of the as-received tape. Therefore, if the surface is smooth, the fatigue life is long. The values of R_a for three kinds of USP tapes are 0.83 μm - 0.88 μm, which are slightly larger than that of the as-received tape. As observed in Fig. 2, the fatigue life of USP tapes is longer than that of the as-received tape. Compressive residual stresses are induced in the surface layer of the material by USP [8]. Although the surface roughness increases slightly by USP, the influence of USP-induced surface roughness on the fatigue life is slight. The reason why the USP-induced surface roughness has a small influence on the fatigue life must be due to compressive residual stresses induced by USP in the surface layer of the tape. The values of residual stress measured were among -80 MPa and -160 MPa in the region of depth from the surface to 200 μm for both the as-received tape and USP tapes. The difference of the residual stresses among the as-received tape and USP tapes was not clearly detected. This reason may be surmised as follows. The tapes were subjected to high work hardening during the rolling process to produce them and therefore high residual stresses were already induced in the material. The detail of the residual stress is the future work.

4. Conclusions

The TiNi SMA tapes showing superelasticity were USP-treated, in which both flat surfaces were shot-peened from two opposite directions, and the influence of shot media diameter and coverage on the fatigue life of alternating-plane bending was investigated. The results obtained are summarized as follows.

1. The larger the bending strain amplitude, the shorter the fatigue life is. The fatigue life can be expressed by a power function of strain amplitude. The fatigue of USP-treated tapes is longer than that of the as-received tape. The fatigue lives of both tapes USP-treated with different shot media diameters at the same coverage are almost the same. The fatigue life of the tape USP-treated with high coverage for the same shot media diameter is longer than that with low coverage.
2. The fatigue crack nucleates at the central part of the flat surface of the tape in the case of the as-received tape. The fatigue crack nucleates at the corner near the flat surface of the tape in the case of the USP-treated tape. The average fatigue crack growth rate decreases by the USP treatment.
3. The hardness on the surface of the tape increases by the USP treatment. The fatigue life increases in proportion to the hardness on the surface of the tape for each bending strain amplitude. The fatigue life can be expressed by an exponential function of Vickers hardness.
4. The surface roughness increases slightly by the USP treatment. The fatigue life of polished and USP-treated tapes is longer than that of the as-received tape.
5. In practical applications of SMAs, the fatigue life of SMA elements increases if USP is treated not only on the surface at the maximum stress point but also on the surface in the region near the maximum stress point.

Acknowledgment

The experimental work for this study was carried out with the assistance of students in Aichi Institute of Technology, to whom the authors wish to express their gratitude. The authors

also wish to extend thanks to the administrators of Scientific Research (C) (General) in Grants-in-Aid for Scientific Research by the Japan Society for Promotion of Science for financial support.

REFERENCES

1) K. Otsuka and C.M. Wayman, eds., Shape Memory Materials, Cambridge University Press, Cambridge, pp. 1-49, 1998.
2) T. Sakuma, U. Iwata and Y. Kimura, Cyclic Behavior and Fatigue Life of TiNiCu Shape Memory Alloy, FATIGUE '96, 1, pp. 173-178, 1996
3) T. Sawaguchi, G. Kaustrater, A. Yawny, M. Wagner and G. Eggeler, Crack initiation and propagation in 50.9 at. pct Ni-Ti pseudoelastic shape-memory wires in bending-rotation fatigue, Metallurgical and Materials Transactions A, 34A, pp. 2847-2860, 2003.
4) M. Wagner, T. Sawaguchi, G. Kaustrater, D. Hoffken and G. Eggeler, Structural fatigue of pseudoelastic NiTi shape memory wires, Materials Science and Engineering A, 378, pp. 105-109, 2004.
5) R. Matsui, H. Tobushi, Y. Furuichi and H. Horikawa, Tensile Deformation and Rotating-Bending Fatigue Properties of a Highelastic Thin Wire, a Superelastic Thin Wire, and a Superelastic Thin Tube of NiTi Alloys, Trans. ASME, J. Eng. Mater. Tech., 126, pp. 384-391, 2004.
6) H. Tobushi, R. Matsui, K. Takeda and E.A. Pieczyska, Mechanical Properties of Shape Memory Materials, Part 2. Fatigue properties of shape memory alloy, Nova Science Pub., New York, pp. 115-164, 2013.
7) L. Wagner ed. Shot peening, Wiley-VCH, Weinheim, pp. 1-562, 2003.
8) S.K. Cheong, D.S. Lee, J.H. Lee, M. Handa and Y. Watanabe, Effect Of Ultrasonic Shot Peening on The Fatigue Characteristics of Welded Sts304 for Rolling Stock, Proc. ICSP-10, pp. 494-498, 2008.
9) H. Tobushi, K. Mitsui, K. Takeda, K. Kitamura and Y. Yoshimi, Performance and Design of Precision-Cast Shape Memory Alloy Brain Spatula, J. Theoretical and Appl. Mech., 50-3, pp. 855-869, 2012.
10) K. Takeda, H. Tobushi, K. Miyamoto and E.A. Pieczyska, Superelastic Deformation of TiNi Shape Memory Alloy Subjected to Various Subloop Loadings, Mater. Trans., 53-1, pp. 217-223, 2012.
11) H. Tobushi, T. Nakahara, Y. Shimeno and T. Hashimoto, Low-Cycle Fatigue of TiNi Shape Memory Alloy and Formulation of Fatigue Life, Trans. ASME, J. Eng. Mater. Tech., 122, pp. 186-191, 2000.
12) E.A. Pieczyska, S. Gadaj, W.K. Nowacki, K. Hoshio, Y. Makino and H. Tobushi, Characteristics of energy storage and dissipation in TiNi shape memory alloy, Sci. Tech. Advanced Mater., 6, pp. 889-894, 2005.
13) R. Matsui, Y. Makino, H. Tobushi, Y. Furuichi and F. Yoshida, Influence of Strain Ratio on Bending Fatigue Life and Fatigue Crack Growth in TiNi Shape-Memory Alloy Thin Wires, Mater. Trans., 47-3, pp. 759-765, 2006.
14) K. Tanaka, T. Hayashi, Y. Ito and H. Tobushi, Analysis of thermomechanical behavior of shape memory alloys, Mech. Mater., 13, pp. 207-215, 1992.
15) K. Takeda, K. Mitsui, H. Tobushi, N. Levintant-Zayonts and S. Kucharski, Influence of Nitrogen Ion Implantation on Deformation and Fatigue Properties of TiNi Shape Memory Alloy Wire, Arch. Mech. 65-5, pp. 391-405, 2013.
16) J.E. Shigley and C.R. Mischke, 5th ed., Mechanical Engineering Design, McGraw-Hill, New York, pp. 282-283, 1989.